Nanoscale

Accepted Manuscript

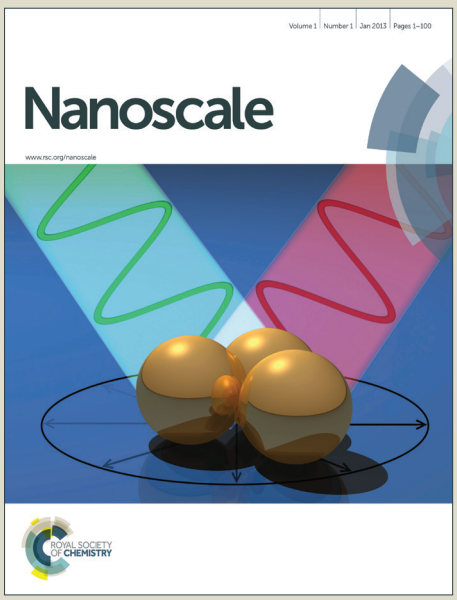

This is an *Accepted Manuscript*, which has been through the Royal Society of Chemistry peer review process and has been accepted for publication.

Accepted Manuscripts are published online shortly after acceptance, before technical editing, formatting and proof reading. Using this free service, authors can make their results available to the community, in citable form, before we publish the edited article. We will replace this *Accepted Manuscript* with the edited and formatted *Advance Article* as soon as it is available.

You can find more information about *Accepted Manuscripts* in the Information for Authors.

Please note that technical editing may introduce minor changes to the text and/or graphics, which may alter content. The journal's standard Terms & Conditions and the Ethical guidelines still apply. In no event shall the Royal Society of Chemistry be held responsible for any errors or omissions in this *Accepted Manuscript* or any consequences arising from the use of any information it contains.

ROYAL SOCIETY OF CHEMISTRY

www.rsc.org/nanoscale

Journal Name

Nanoscale

Dynamic Article Links ►

Cite this: DOI: 10.1039/c0xx00000x

www.rsc.org/xxxxxx

ARTICLE TYPE

Tuning nanowire growth mode via the interaction among seed, substrate and beam fluxes

Valentina Zannier [a,b], Vincenzo Grillo [c,d], Faustino Martelli [e], Jasper Rikkert Plaisier [f], Andrea Lausi [f] and Silvia Rubini*[a]

Received (in XXX, XXX) Xth XXXXXXXXX 20XX, Accepted Xth XXXXXXXXX 20XX
DOI: 10.1039/b000000x

The growth mechanism of semiconductor nanowires is still an argument of high interest, becoming clearer, investigation after investigation, that simple pictures fail to describe the complex behaviors observed under different growth conditions. We report here on the growth of semiconductor nanowires maintaining the control over the chemical composition and the physical state of the metallic seed, and tuning the growth mechanism by varying the growth conditions. We focused on Au-assisted ZnSe nanowires grown by molecular beam epitaxy on GaAs(111)B substrates. We show that, at sufficiently high temperatures, the Au seed is strongly affected by the interaction with the substrate and that the nanowires growth can occur through two different mechanism, having a strong impact on nanowires morphology and crystal quality. In particular, ZnSe NWs may exhibit either a uniformly oriented, straight morphology when the nanoparticle seed is liquid, or a kinked, worm-like shape when the seed nanoparticle is switched in the solid phase. This switch, that tunes the nanowires growth mechanism, is obtained by controlling the Zn-to-Se beam pressure ratio at the Au-seed surface. Our results allow a deeper understanding of particle-assisted nanowire growth, and an accurate control of nanowires morphology via the control of the growth mechanism.

Introduction

Semiconductor nanowires (NWs) are attracting increasing interest due to the novel properties that make them promising building blocks for electronic and optoelectronic devices.[1-3] The full potentials of these nanostructures, however, will only be realized when a deep understanding and an accurate control of the growth process will be reached. The nanoparticle-assisted bottom-up growth from vapor phase by means of molecular beam epitaxy (MBE) offers the possibility to have the precise control of the growth parameters, which is essential for the achievement of this purpose. In this approach, a metal nanoparticle (NP) seed acts as a collector of atoms from the molecular beams and drives the one-dimensional growth of the semiconductor material. Gold is the most common metal used to assist vapor-phase nanowire growth,[4] and the most widespread method to generate the nanoparticles is dewetting a thin metal film deposited on the substrate. This process results in the formation of particles with size, shape and chemical composition that strongly depend on the nature of the substrate, the interaction between the metal film and the substrate, and the temperature at which this process occurs.[5, 6] The morphology and the physical state of the nanoparticles affect the nanowire growth mechanism, playing a crucial role in determining the properties of the nanowires.[7-9] In addition to the thermal history and the chemical interaction between metal film and substrate, the total vapor pressure and the ratio between the NW-precusors pressures can also affect composition and physical state of the NPs during the growth, dynamically changing the growth mechanism and the resulting wires properties. Kodambaka et al.[10] reported the chemical vapor growth of Ge NWs assisted by Au nanoparticles, showing that the NW growth can occur with either liquid or solid particles at the same temperature, and the seed state depends on the total pressure in the growth chamber. Hillerich et al.[11] reported on the epitaxial growth of InP NWs from Cu NPs by metal-organic vapor phase epitaxy, showing the effect of the P/In pressure ratio on particle composition, NWs growth rate and mechanism. Gamalski et al.[12, 13] showed real time transmission electron microscopy studies of the formation and the evolution of Au seed particles during Ge NWs growth. They found metastable AuGe particles, whose formation involve changes in composition, pointing out the importance of the seed-particle configuration for the subsequent NW growth mechanism. Indeed, those NPs can either recrystallize or remain liquid during NWs growth at the same temperature, depending on the Ge supersaturation, that can be controlled through the precursor partial pressure.

Different growth modes, arising from seed configuration and dynamics changes during the growth, are often reflected in different wire shape and crystal quality.[14, 15] This suggests that growth parameters can be modulated to create the desired structures. For instance, Caroff et al.[16] reported the full control of the crystal structure of InAs NWs by varying wire diameter and growth temperature. Tian et al.[17] also reported the synthesis of a

Nanoscale Accepted Manuscript

kinked nanowire superstructure obtained by an iterative modulation of the gaseous reactant supply. Therefore, studying the effects of sample preparation and growth conditions on the NWs growth mechanism can provide the necessary tools to achieve the control and the tunability of the nanostructure properties.

As for the specific material we have chosen for our investigation, ZnSe, Au-assisted vapor-solid-solid (VSS) growth mechanism has been reported for temperature as high as 510°C on ZnSe[18] or oxidized silicon[19-21] substrates. Similarly, the VSS mechanism for thin ZnSe NWs grown on GaAs(111)B has been reported at 300°C.[21] On the other hand, it is known that some Ga interdiffusion can occur upon annealing Au films at higher temperatures on GaAs substrates, a feature that may affect both seed composition and physical state. Cai et al.[22] reported the growth of ZnSe NWs on GaAs at 530°C, suggesting that the seeds consist of liquid Au-Ga alloy nanoparticles. However, they did not obtain long and uniformly oriented ZnSe NWs, but rather NWs showing a strong diameter-dependent growth direction. The vapor-liquid-solid (VLS) mechanism has also been invoked for the growth of ZnSe NWs with seeds melting at temperatures lower than the growth temperature (T_g), like Ga[23] or Au-Sn[24] and Au-Si[25] intermetallic compounds.

To reach a deeper understanding of the NWs growth, we have performed a detailed investigation of the growth mechanism of Au-induced ZnSe nanowires on GaAs(111)B by molecular beam epitaxy at the fixed T_g of 450°C. As it will be shown in the following, this temperature is indeed sufficiently high to allow interaction of the Au film with the GaAs substrate, but also sufficiently low to give effective growth of ZnSe NWs by MBE.[26] With the help of *in-situ* and *ex-situ* electronic and structural measurements we show that, due to the interplay between substrate, metal, and beam fluxes, both VLS and VSS growth mechanisms may take place at this temperature. The occurrence of one or the other mechanism has an impact on NW morphology and nanoparticle composition, and can be controlled by the growth protocol.

Results and discussion

As briefly mentioned above, the NWs of this work have been grown at 450 °C on GaAs(111)B substrates. The annealing at this T of deoxidized GaAs(111)B substrates covered by 1 nm Au results in the formation of nanoparticles with a size distribution between 15 and 65 nm, and a mean diameter of 30 nm. The subsequent ZnSe deposition at the same temperature leads the growth of ZnSe NWs with the same density and diameter distribution and an almost uniform diameter for the whole length. However, the NWs morphology is strongly affected by the Zn/Se pressure ratio. Figure 1 shows SEM images of ZnSe NWs obtained for 10 minutes deposition using a Zn/Se beam pressure ratio (BPR) of 0.4 (a) and 4 (b), respectively.

Under Se-rich conditions (BPR0.4), disordered and kinked nanowires grow, with a "worm-like" shape and without any preferential growth direction. Increasing the Zn/Se pressure ratio (BPR 4) vertically oriented and straight ZnSe nanowires are obtained. The NP shape is also different, as it can be observed in the insets of Fig. 1 (a, b): faceted NPs, with an irregular profile

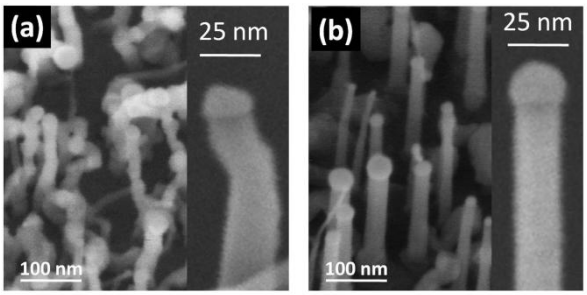

Figure 1 Tilted-view SEM images of ZnSe NWs obtained after 10 minutes deposition at 450°C with BPR 0.4 (Se-rich) (a) and 4 (Zn-rich) (b). The insets are magnified images of representative nanowires shown in the correspondent panels.

are visible on the tips of ZnSe NWs grown with an excess of Se, while spherical NPs are found on the tips of NWs grown under Zn-rich conditions. The differences in NWs morphology and NPs shape suggest that two distinct growth modes take place under the two opposite Zn/Se pressure ratios, even if the NWs length, i.e. the growth rate, is comparable.

Let us now focus our attention on the NPs assisting the growth, and on their interaction with Zn and Se fluxes. In figure 2 we report how XPS and XRD measurements of the Au covered GaAs(111)B substrate are affected by the thermal annealing. In panel 2 (a) we report the XPS spectra of the Au 4f core level measured *in-situ* at RT and after 10 minutes annealing at different temperatures. The $4f_{7/2}$ peak has the same shape and position (BE = 84.00 eV, Δ_{SO} = 3.68 eV) after RT deposition and after annealing at 300°C, tracing the signal of pure metallic Au.[27] Conversely, from 400°C upwards, a progressive shift in the peak position toward higher binding energies is observed. This indicates the occurrence of a chemical interaction between the gold film and the substrate, i.e. the interdiffusion of Ga atoms from the substrate into the Au layer and the formation of a Au-Ga alloy phase, followed by As desorption.[28] The difference in the peak position with respect to that of pure gold reflects the amount of Ga in the alloy, that is greater for higher temperatures.[28, 29] In particular, after the annealing at 450°C the Au $4f_{7/2}$ peak has a binding energy of 84.65 eV. This core-level binding energy could be ascribed to an alloy with a Ga atomic fraction of 0.33 or slightly less if nanometer-sized clusters are measured in spite of bulk alloys.[28] Based on the Au-Ga binary system,[30] Au-Ga alloys with a Ga mole fraction in the range between 0.22 and 0.45 are in the molten state at 450°C. This suggests the presence of liquid Au-Ga alloy instead of solid Au at the surface of the nanoparticles. However, the limited escape depth of the XPS technique (λ=1.5 nm in our setup) prevents us to discriminate between the formation of nanoparticles with homogeneous composition and a limited surface alloying. In order to verify the physical state and the phase transition of the Au nanoparticles due to alloying with Ga during annealing, Au-covered samples were analyzed by grazing incidence XRD as a function of the annealing temperature. In figure 2 (b) we report the XRD powder spectra at different temperatures, within the 2θ range in which the most intense signals of Au are expected. We did not get any powder diffraction pattern at low temperature because of the epitaxial nature of the metal film deposited on deoxidized GaAs(111)B.[31] The dewetting process begins to be effective at

Nanoscale Accepted Manuscript

This journal is © The Royal Society of Chemistry [year]

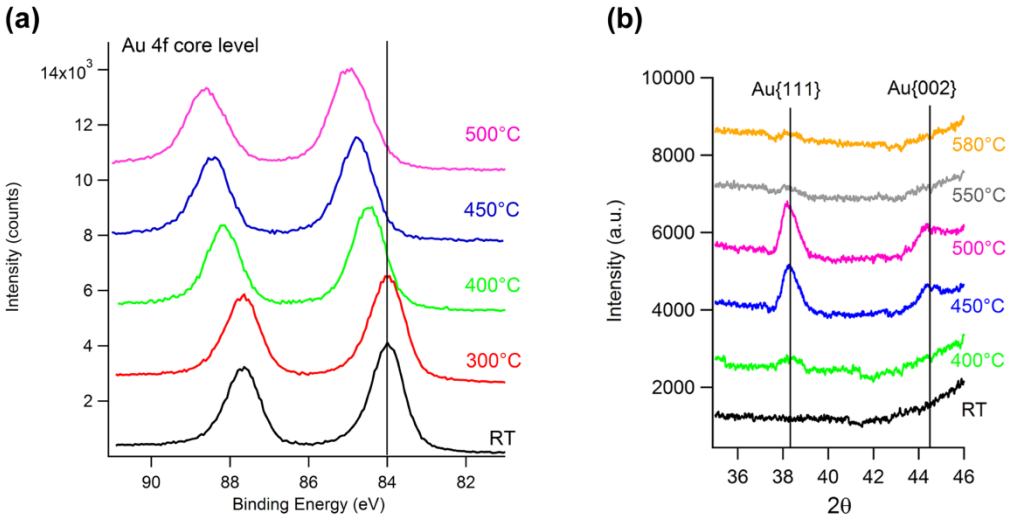

Figure 2 (a) XPS spectra of the Au 4f core level of the metal film deposited on GaAs(111)B at room temperature and after annealing at the different temperatures reported in the panels. The line at 84.00 eV indicates the position of the $4f_{7/2}$ peak of pure Au. A clear blue-shift of the binding energy of the 4f core level electrons is observed, which indicates an increasing interaction of the Au metal film with the GaAs substrate. (b) Grazing incidence XRD patterns of the nanoparticles as a function of temperature. The Au diffraction peaks are detected up to 550°C, when they disappear, suggesting the melting of the NPs.

400°C when the Au diffraction peaks weakly appear. The intensity of the diffraction peaks increases at 450°C and the signals are well detectable up to 550°C, when they disappear, suggesting the melting of the nanoparticles.

The diffraction peaks are quite broad, because of the nanometer-sized diameter of the nanoparticles. Due to this broadening, and to the close similarity between the lattice constant of gold and of gold-rich solid Au-Ga solutions,[31, 32] the distinction between these two phases has not been possible. However, a solid phase is clearly present up to 550°C. Such phase could be either pure gold or a gold-gallium solid solution with a Ga molar fraction smaller than 0.22.[30]

Combining the results of XPS and XRD analysis, we can speculate that the metal NPs obtained by dewetting the Au film on GaAs(111)B at 450°C have a liquid Au-Ga alloy shell, and a solid core made of pure Au or Au-rich solid solution. This picture is supported by the theoretical study by Kratzer et al.[33] about energetics of As, Ga and Au(111) as a model system for gold NPs involved in the growth of GaAs NWs. They demonstrated that the coexistence of a Ga-Au surface solution and an ordered phase of Au_7Ga_2 in the catalyst particle is likely, since the formation of Ga substitution in the topmost layers is more favorable than in the subsurface Au layers. Although they considered Ga atoms impinging from gas phase, the tendency to form a surface alloy due to the lower diffusion barrier and the lower formation energy for Au-Ga alloy at the NP surface can be also supposed in the case of Ga atoms coming from the substrate.

It is worth noting that the size distribution of the NPs is quite broad, thus their composition and their physical state at the same temperature could be not the same for all of them. For instance, smaller NPs could have an homogeneous composition and be completely liquid at 450°C, whereas bigger ones could have a inhomogeneous phase, with Ga concentration decreasing from the surface to the center. Tchernycheva et al.[8] showed in situ RHEED and TEM evidences of Au NPs phase transition during the annealing of a thin gold film on GaAs(111)B. They reported the range between 340 and 400°C as the phase transition temperature window in which the complete melting of Au-Ga alloy NPs with diameters from 5 to 15 nm is observed. Moreover, they found a size-dependent composition of the re-crystallized particles under As-flux, suggesting that the amount of Ga into the NPs, i.e their composition, depends both on substrate temperature and particle size. We believe that also in our case the composition of the NPs obtained at 450°C could be size-sensitive, thus some of them could be liquid (most probably the smallest) and some others could have a liquid shell and a Au-rich solid core.

The impact of Se and Zn beams on the chemical composition of the Au-Ga alloy NPs is revealed by the analysis of the NPs morphology and the Au 4f core-level emission after exposing the annealed samples to the individual fluxes. Figure 3 shows the SEM images of the NPs after dewetting (a) and after exposing the annealed samples at Zn (b) or Se (c) fluxes for 1 minute at 450°C. Fig. 3(d) displays the corresponding Au 4f core-level spectra.

The Zn beam does not alter the chemical composition of the Au-Ga NPs, as suggested by the Au 4f peak position, which is the same before and after the Zn exposure ($Au4f_{7/2}$ = 84.65 eV). The morphology of the resulting NPs (Fig. 3 (b)) is also very similar to that of the NPs shown in Fig. 3 (a), obtained by annealing the Au-covered sample at 450°C without any Zn or Se beams. Conversely, the Au 4f peak of the NPs exposed to Se beam is back-shifted to a binding energy of 84.00 eV, that is the metallic gold peak position. The SEM image of such NPs (Fig. 3(c)) shows some relevant differences: the particles are more faceted, and a step underneath them is clearly visible. Furthermore, they have a different image contrast, suggesting a different electrical and chemical composition.

These results suggest that the Se beam reacts with Ga atoms of the Au-Ga alloy NPs, giving a Ga_xSe_y solid compound that precipitates and leaves behind pure Au nanocrystals.

When ZnSe nanowires grow, Zn and Se beams are simultaneously supplied on the Au-Ga alloy NPs. After 1 minute of ZnSe deposition at BPR 4, the Au $4f_{7/2}$ peak is still centered at

Nanoscale Accepted Manuscript

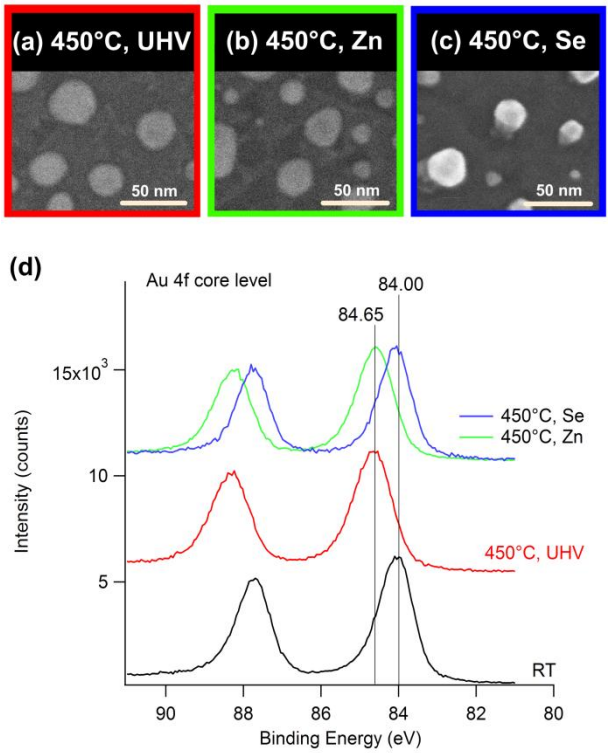

Figure 3 Morphology and XPS spectra of the Au NPs after their interaction with the GaAs substrate at 450°C and after their interaction with Zn or Se fluxes. (a), (b) and (c):SEM images of the Au NPs annealed in ultra-high vacuum (red frame), after the interaction with the Zn flux (green frame) or after the interaction with the Se flux (blue frame). The same color code is used to show the XPS spectra in the lower panel (d): The red curve indicates an increase of the binding energy of the Au 4f electrons when the temperature (450 °C) allows the Au film to interact with the substrate (compare with the black curve taken at room temperature); no further change is observed when the annealed NPs interact with the Zn flux (green curve), while the original binding energy is recovered when the annealed NPs interact with the Se flux (blue curve).

84.65 eV, whereas after the same deposition time at BPR 0.4 it is back-shifted toward the pure gold position.[†] The picture that emerges from the data is sketched in Fig. 4(a) that describes the core of our work: under Zn-rich conditions (BPR 4), the supplied Se mainly reacts with Zn atoms to give the ZnSe crystal, and the one-dimensional growth is promoted by liquid Au-Ga alloy NPs, or solid Au-rich particles surrounded by a liquid Ga-rich shell (VLS mode). On the other hand, when the Au-Ga alloy NPs are exposed to Se-rich vapors (BPR 0.4), the excess of Se reacts with Ga atoms, depleting the alloy particles and making them solidify at the very beginning of the deposition. The NWs growth proceeds now assisted by Au solid nanocrystals (VSS mode). Indeed the Au-Zn[34] and the Au-Se[35] binary systems show only high-temperature melting compounds, and even if the melting point could be lowered due to size-effects,[36] this is not playing a significant role in our case, since the difference between the lowest eutectic temperature (659°C) and the NWs growth temperature (450°C) is too large.

We thus believe that, as soon as the Se beam reacts with Ga atoms of the Au-Ga alloy droplets, the NPs become solid and remain solid during the NWs growth. Au assisted vapor-solid-solid growth of ZnSe NWs on ZnSe substrate at temperature as high as 500°C has been indeed recently reported.[18]

The different wires morphology obtained with the two opposite BPR results from the two different growth mechanism, as also schematically illustrated in Fig. 4(a). It is widely known that growth from solid seed particles often suffers from the problem of a less controlled growth direction.[4, 37] Solid particles are less uniform in shape and may have varying facets, producing nanowires with a less uniform shape. On the contrary, liquid NPs, or a liquid shell around the NPs, may provide a more uniform and isotropic medium for NW nucleation and growth. Moreover, the diffusivity through a liquid particle is usually faster than that through a solid particle, hence the probability for the impinging atoms to find a nucleation site before reaching the nanoparticle-nanowire interface, leading a change in the growth direction, is higher for solid NPs. This results indeed in the growth of kinked NWs, as it occurs when ZnSe NWs are grown under Se-rich conditions. On the other hand, the liquid state of the surface layers alone may not be sufficiently efficient to give a measurably faster growth rate.

High-resolution TEM images of the NWs tips are shown in Figure 4 (b) and (c). Lattice structure and parameter of the faceted NP of figure 4(b), on the tip of a worm-like ZnSe NW grown under excess of Se, is consistent with that of Au fcc crystal. A significant amount of particles containing two crystal grains are found on the tips of these wires, both having the lattice parameter of fcc Au.[†] The presence of two grains may be due to the coexistence at 450° C of two phases (the Au solid core and the Au-Ga liquid alloy shell) and the subsequent fast solidification of the liquid phase due to the Ga removal. On the other hand, most of the spherical shaped NPs found on the tips of Zn-rich grown NWs (Figure 4 (c)) have a lattice non compatible with a pure Au phase, but rather close to the Au_7Ga_2 hexagonal compound.

STEM-EDX analysis of several ZnSe NWs reveals the presence of 7-15 % of Ga, averaged on the NP volume, on the tips of Zn-rich grown NWs (Fig. 4 (e)). In the NPs of Se-rich grown wires (Fig. 4 (d)) this value drops below 5%, close to our detection limit.

The NWs body consists of stoichiometric ZnSe for both kinds of wires. NWs grown under Zn rich conditions have a wurtzite crystal structure with the *c* axes parallel to the growth direction for the whole length, whereas wires grown at BPR 0.4 also have a wurtzite crystal structure, but with a higher density of stacking faults and an ill-defined growth direction. Moreover, their interface with the NP is rarely flat and perpendicular to the growth direction.

Nanowires growth through different growth mechanisms at the same temperature has been already reported for other systems. For instance Heun et al.[38] suggest the coexistence of VLS and VSS growth in Pd-assisted InAs NWs grown by chemical beam epitaxy; Kodambaka et al.[10] also reported the presence of both solid and liquid seed particles during Ge NWs growth, observed by *in-situ* TEM. Hillerich et al.[11] showed the simultaneous growth of two types of InP NWs side by side on the same substrate, assisted by solid Cu_2In and liquid In-rich particles respectively. In all those systems the NP properties (diameter,

Nanoscale Accepted Manuscript

This journal is © The Royal Society of Chemistry [year]

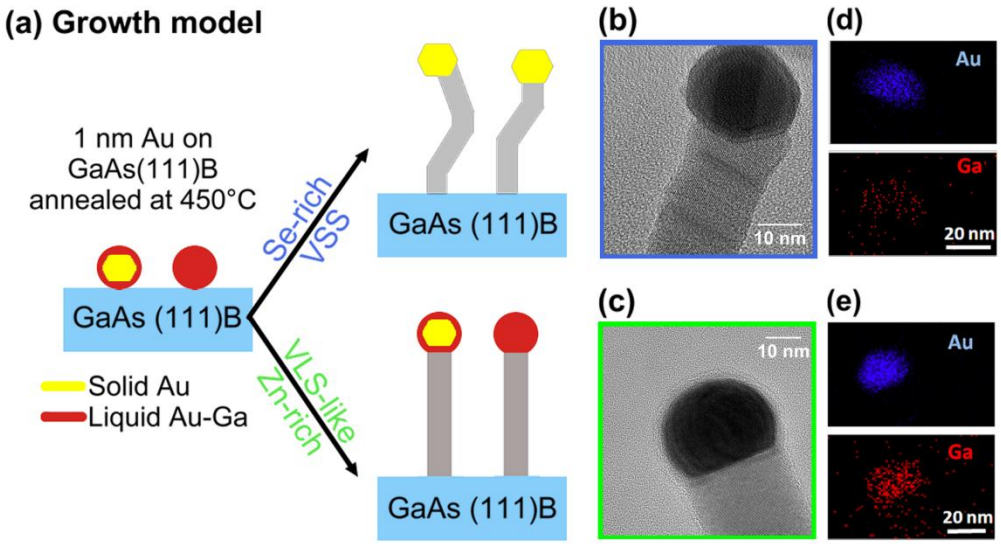

Figure 4 (a) Schematic view of the BPR-dependent ZnSe NWs growth mechanisms. The thermal dewetting of the Au film on GaAs(111)B leads the formation of Au-Ga alloy nanoparticles that could be either totally liquid, or solid with a liquid shell. Using Se-rich conditions, the excess of Se reacts with the alloy nanoparticles, draining out Ga atoms and making them solidify. The NWs growth goes on assisted by solid Au nanocrystals (VSS mode), leading the formation of kinked ZnSe NWs. On the other hand, using Zn-rich conditions, all the Se supplied reacts with the Zn beam, therefore the growth is assisted by Au-Ga alloy NPs in the VLS-like mode, that leads the growth of straight and uniformly oriented NWs. (b, c) HRTEM images and (d, e) EDX elemental maps of the NPs on the tips of two ZnSe NWs grown under Se-rich (b, d) and Zn-rich (c, e) conditions respectively.

thermal history, chemical composition) make the difference. The occurrence of one or the other mechanism, depending on the NP composition is a very attractive issue that suggests the possibility to select the wires properties through the control of the dynamic process happening inside or at the surface of the nanoparticle. For the system studied in this work, the Se-induced changes in the NPs composition allow us to choose the growth mechanism and, in case, change the NWs morphology during the growth. Figure 5 shows ZnSe NWs grown for 15 minutes in Zn-rich conditions and, after a rapid BPR switch, by further 15 minutes growth under excess of Se.

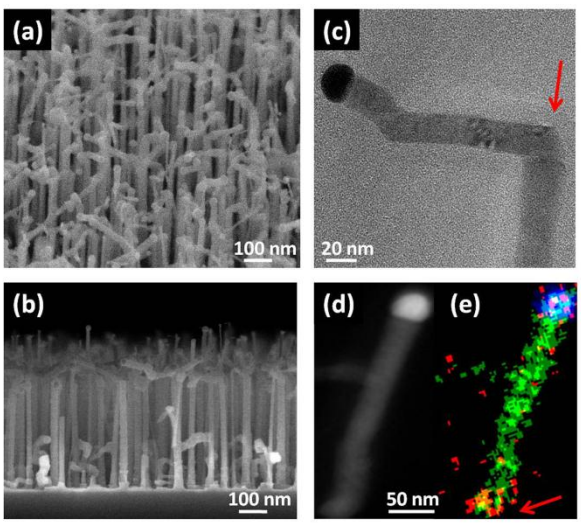

Figure 5 (a, b) Tilted-view and crossed-view SEM images of ZnSe NWs grown for 15 minutes at BPR 4 followed by 15 minutes at BPR 0.4. (c) TEM image of a nanowire in which the two portions grown under opposites conditions are clearly visible. (d, e) STEM and EDX map of a NW broken at the BPR change point, i.e. at the kink. Colors index: Zn K: light green; Se K: dark green; Au M: blue; Ga K: red. The red arrows indicate the BPR switch point.

Similar results are also obtained if the growth occurs under Zn-rich condition for the whole time, but a 1 minute-long interruption of the Zn flux is provided at any moment of the growth (not shown). In both cases, as soon as the Au-Ga alloy NPs undergo an excess of Se, with the ensuing reaction of Ga with Se and the sudden solidification of the nanoparticle, the wire kinks. Afterwards, the growth goes on lead by a solid Au particle towards the formation of a worm-like upper part of the NW. An excess of Ga can be detected by EDX at the BPR switch point, suggesting the effectiveness of such mechanism (Fig. 5 (d,e)).

On the other hand, if we maintain Zn-rich conditions for the whole deposition time, the growth of uniformly straight and long ZnSe NWs is achieved (see Figure 6 (a)), with spherical Au-GaNPs on their tips. If these NWs are then exposed only to Se flux for few minutes at the end of the growth, the NPs on their tips change shape and composition (see Figure 6 (b)), becoming pure Au faceted nanocrystals. The depletion from Ga of Au-Ga nanoparticles following after-growth exposure to As was already observed in the case of GaAs NWs.[39, 40] The purification of the NP was accompanied by the formation of a GaAs "neck" due to the reaction of Ga atoms from the nanoparticle with the As beam. Interestingly, in our case such "Se-purified" NPs show a diameter-dependent crystal structure: small particles are regular multiply twinned icosahedral nanoparticles (MTPs), while large NPs are fcc crystals still containing twin boundaries (Figure 6 (c), (d)). It is known that MTPs are regular structures that form upon rapid quenching from liquid and are stable up to about 15 nm diameter.[41-43] As the size of a cluster increases, these structures become less favorable due to accumulated strain energy, therefore bigger nanoparticles crystallize into the more stable fcc structure with some residual twins. The presence of icosahedral gold particles at the tips of these nanowires indirectly confirms that the seed NPs were in the liquid state during the growth, becoming

Nanoscale Accepted Manuscript

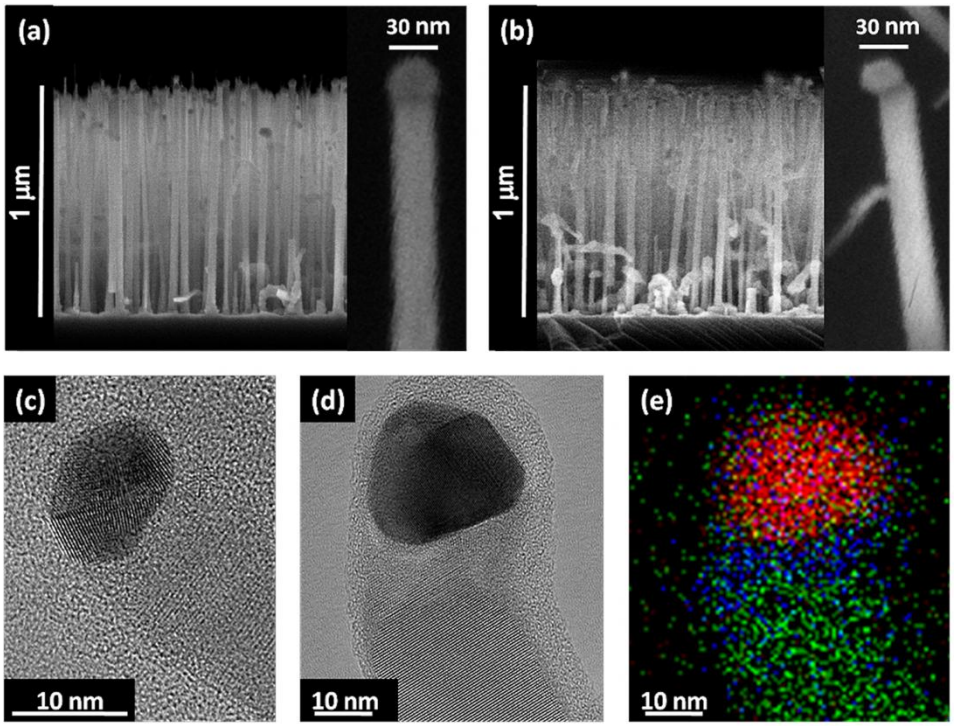

Figure 6 (a) ZnSe nanowires grown at BPR 4 (Zn-rich) for 30 minutes. (b) The same wires kept for 1 minute under Se flux at the end of the growth. The insets on the right are magnified SEM images of transferred nanowires, in which the different nanoparticle shape is clearly visible. (c, d) HRTEM images of two NWs of the sample shown in panel (b), having a different diameter and a different NP crystal structure: multiply twinned icosahedral nanoparticles (MTP) (c) and fcc (d). (e) EDX map of the wire shown in (d). Au M: red, Ga K: blue, Zn K: green.

solid as the Se beam alone is supplied, due to the fast depletion from Ga atoms. Moreover, a neck between the particle tip and the NW body is obtained after this treatment (Figure 6 (d)). This neck is mainly crystalline but with variable spacing and orientation, and the EDX map shows a heap of gallium therein (Figure 6 (e)). We cannot exclude that a slow release of Ga from the NP to the NW body may take place also during growth in Zn-rich condition, giving a distribution of Ga impurities in the NW body below the detection limit of EDX measurements. As a matter of fact, the extremely good alignment of NWs observed in Fig. 6(a) get progressively worse in case of growth longer than 1.5 um (not shown) suggesting a progressive depletion of the NP and solidification of the shell.

Conclusions

In this work we have shown that, provided the necessary thermal budget, an interplay between seed-substrate interaction and elemental fluxes supply occurs. Based on this, we can tune the NW growth mechanism from being VLS-based to become VSS-like. In particular we have shown that the thermal diffusion of Ga atoms from the substrate into the Au seed NPs leads to the formation of liquid Au-Ga alloy at the NP surface. The chemical composition and the physical state of such NPs are strongly affected by the Se flux. Therefore, using Zn-rich conditions, the growth of ZnSe NWs occurs through the VLS growth mode, assisted by Au-Ga alloy droplets that could be either completely liquid or solid with a liquid shell. On the other hand, if Se-rich conditions are used, the NWs growth mechanism is switched toward the VSS mode, assisted by solid Au nanocrystals. The growth mechanism has a profound impact on the NW morphology and crystal quality. Indeed, at high Zn/Se ratio straight and uniformly oriented ZnSe NWs are obtained, whereas at low Zn/Se ratio kinked and worm-like NWs grow. In the former case the crystal structure of the NW results of higher quality with a strongly reduced density of defects, the WZ phase dominating in the NWs in both cases. These results constitute an interesting example of how alloyed foreign metal particles, as in this case Au-Ga NPs obtained by annealing of Au on GaAs, and preserved by growth under Zn-rich conditions, may be optimal for the growth of semiconductor NWs, as recently suggested by Dick et al.[44] We have shown that the switch from one growth mechanism to the other is possible within a single growth and that this change has immediate effects on the wires morphology. Furthermore, we have demonstrated that different growth terminations affect chemical composition and crystal structure of the nanoparticles on the nanowires tips.

The conclusions of this work have been deduced by experiment on ZnSe NWs but we are convinced that they are valid in all systems where the interaction of the seed with the substrate and the beam fluxes induces changes in the physical state of the NPs.

Experimental

ZnSe nanowires were grown by solid source molecular beam epitaxy (MBE) in a multi-chamber ultra-high-vacuum facility. The GaAs(111)B substrates were first deoxidized at 600°C in the III – V chamber. A 1 nm thick Au layer was deposited at room

Nanoscale Accepted Manuscript

This journal is © The Royal Society of Chemistry [year]

temperature in the metallization chamber and then the samples were transferred into the II – VI growth chamber where 10 minutes annealing at 450°C were followed by ZnSe deposition at the same temperature. We used elemental Zn and Se sources, fluxes corresponding to a two-dimensional ZnSe growth rate of 0.5 μm/h at 280°C, and a Zn-to-Se beam pressure ratio (BPR) of 0.4 (Se-rich conditions) and 4 (Zn-rich conditions). The Au film dewetting process during the annealing was studied by *in-situ* x-ray photoemission spectroscopy (XPS) and *ex-situ* grazing-incident x-ray diffraction (XRD). The XPS analysis was carried out before and after the annealing in the Al-Kα photoemission chamber connected to the MBE system, whereas powder XRD patterns were collected as a function of the annealing temperature at the MCX beamline of Elettra synchrotron radiation source, operating at 8 KeV and equipped with a furnace end-station.[45] The morphology of the ZnSe nanowires was characterized using a Zeiss SUPRA40 Scanning Electron Microscope (SEM). Trasmission Electron Microscopy (TEM) was performed using a JEOL 2200 operated at 200 KeV and with a Scherzer resolution in TEM and scanning TEM (STEM) of 0.19 nm and 0.14 nm respectively. The microscope is equipped with EDX and Ω-filter for energy loss analyses.

Notes and references

[a] *IOM-CNR Laboratorio TASC, S.S. 14, Km 163.5, I-34149 Trieste, Italy Fax: +39 040226767; Tel: +39 0403756437; E-mail: rubini@iom.cnr.it*
[b] *PhD School of Nanotechnology, Department of Physics, University of Trieste, via Valerio 2, I-34127 Trieste, Italy*
[c] *IMEM-CNR, Parco Area delle Scienze 37/A, I-43010 Parma, Italy S3*
[d] *NANO-CNR, Via Campi 213/A, I-41125 Modena, Italy*
[e] *IMM-CNR, via del Fosso del Cavaliere 100, I-00133 Roma, Italy*
[f] *SincrotroneTrieste S.C.p.A., Elettra Laboratory, S.S. 14, Km 163.5, I-34149 Trieste, Italy*

† Electronic Supplementary Information (ESI) available: See DOI: 10.1039/b000000x/

1. R. Agarwal and C. M. Lieber, *Applied Physics A*, 2006, **85**, 209–215.
2. R. Yan, D. Gargas, and P. Yang, *Nature Photonics*, 2009, **3**, 569–576.
3. P. Yang, R. Yan, and M. Fardy, *Nano letters*, 2010, **10**, 1529–36.
4. M. E. Messing, K. Hillerich, J. Johansson, K. Deppert, and K. A. Dick, *Goldbulletin*, 2009, **42**, 172–181.
5. M. C. Plante, J. Garrett, S. C. Ghosh, P. Kruse, H. Schriemer, T. Hall, and R. R. LaPierre, *Applied Surface Science*, 2006, **253**, 2348–2354.
6. a. Rath, J. K. Dash, R. R. Juluri, a. Rosenauer, M. Schoewalter, and P. V. Satyam, *Journal of Applied Physics*, 2012, **111**, 064322.
7. M. E. Messing, K. Hillerich, J. Bolinsson, K. Storm, J. Johansson, K. a. Dick, and K. Deppert, *Nano Research*, 2010, **3**, 506–519.
8. M. Tchernycheva, J. C. Harmand, G. Patriarche, L. Travers, and G. E. Cirlin, *Nanotechnology*, 2006, **17**, 4025–30.
9. S. C. Ghosh, P. Kruse, and R. R. LaPierre, *Nanotechnology*, 2009, **20**, 115602.
10. S. Kodambaka, J. Tersoff, M. C. Reuter, and F. M. Ross, *Science*, 2007, **316**, 729–32.
11. K. Hillerich, K. A. Dick, M. E. Messing, K. Deppert, and J. Johansson, *Nano Research*, 2012, **5**, 297–306.
12. A. D. Gamalski, J. Tersoff, R. Sharma, C. Ducati, and S. Hofmann, *Nano letters*, 2010, **10**, 2972–6.
13. A. D. Gamalski, J. Tersoff, R. Sharma, C. Ducati, and S. Hofmann, *Physical Review Letters*, 2012, **108**, 255702.
14. P. Madras, E. Dailey, and J. Drucker, *Nano letters*, 2009, **9**, 3826–3830.
15. M. Kolíbal, T. Vystavel, P. Varga, and T. Sikola, *Nano letters*, 2014, Just Accepted Manuscript. DOI: 10.1021/nl404159x.
16. P. Caroff, K. A. Dick, J. Johansson, M. E. Messing, K. Deppert, and L. Samuelson, *Nature nanotechnology*, 2009, **4**, 50–55.
17. B. Tian, P. Xie, T. J. Kempa, D. C. Bell, and C. M. Lieber, *Nature nanotechnology*, 2009, **4**, 824–9.
18. E. Bellet-Amalric, M. Elouneg-Jamroz, P. Rueda-Fonseca, S. Bounouar, M. Den Hertog, C. Bougerol, R. André, Y. Genuist, J. P. Poizat, K. Kheng, J. Cibert, and S. Tatarenko, *Journal of Crystal Growth*, 2013, **378**, 233–237.
19. A. Colli, S. Hofmann, A. C. Ferrari, C. Ducati, F. Martelli, S. Rubini, S. Cabrini, A. Franciosi, and J. Robertson, *Applied Physics Letters*, 2005, **86**, 153103.
20. J. Basu, R. Divakar, J. Nowak, S. Hofmann, A. Colli, A. Franciosi, and C. B. Carter, *Journal of Applied Physics*, 2008, **104**, 064302.
21. V. Zannier, F. Martelli, V. Grillo, J. R. Plaisier, A. Lausi, and S. Rubini, *Physica Status Solidi RRL*, 2014, **8**, 182–186.
22. Y. Cai, S. K. Chan, I. K. Sou, Y. F. Chan, D. S. Su, and N. Wang, *Advanced Materials*, 2006, **18**, 109–114.
23. Y. Liang, Y. Tao, and S. K. Hark, *CrystEngComm*, 2011, **13**, 5751.
24. K. B. Kahen, I. A. Goldthorpe, and J. Minter, *Journal of Crystal Growth*, 2011, **322**, 57–62.
25. C. Fernandes, H. Ruda, A. Saxena, and C. De Souza, *Physica Status Solidi (C)*, 2012, **9**, 2460–2464.
26. K. Imai, K. Kumazaki, T. Haga, and Y. Abe, *Journal of Crystal Growth*, 1988, **91**, 617–622.
27. P. Citrin, G. Wertheim, and Y. Baer, *Physical Review Letters*, 1978, **41**, 1425–1428.
28. G. Petro, T. Kendelewicz, I. Lindau, and W. E. Spicer, *Physical Review B*, 1986, **34**, 7089–7106.
29. J. A. Nicholson, J. D. Riley, R. C. G. Leckey, J. G. Jenkin, J. Liesegang, and J. Azoulay, *Physical Review B*, 1978, **18**, 2561–2567.
30. J. Liu, C. Guo, C. Li, and Z. Du, *Journal of Alloys and Compounds*, 2010, **508**, 62–70.
31. S. Leung and A. G. Milnes, *Thin Solid Films*, 1983, **104**, 109–131.
32. D. D. L. Chung and E. Beam III, *Thin Solid Films*, 1985, **128**, 299–319.
33. P. Kratzer, S. Sakong, and V. Pankoke, *Nano letters*, 2012, **12**, 943–948.
34. H. S. Liu, K. Ishida, Z. P. Jin, and Y. Du, *Intermetallics*, 2003, **11**, 987–994.
35. T. B. Massalski, *Binary Alloy Phase Diagrams*, ASM International, Materials Park, Ohio, 2nd edn., 1990, vol. 1
36. P. Buffat and J-P. Borel, *Physical Review A*, 1976, **13**, 2287–2298.
37. S. V. Thombare, A. F. Marshall, and P. C. McIntyre, *Journal of Applied Physics*, 2012, **112**, 054325.
38. S. Heun, B. Radha, D. Ercolani, G. U. Kulkarni, F. Rossi, V. Grillo, G. Salviati, F. Beltram, and L. Sorba, *Small*, 2010, **6**, 1935–41.
39. J. C. Harmand, G. Patriarche, N. Péré-Laperne, M.-N. Mérat-Combes, L. Travers, and F. Glas, *Applied Physics Letters*, 2005, **87**, 203101.
40. A. I. Persson, M. W. Larsson, S. Stenström, B. J. Ohlsson, L. Samuelson, and L. R. Wallenberg, *Nature materials*, 2004, **3**, 677–81.
41. Y. G. Chushak and L. S. Bartell, *The Journal of Physical Chemistry B*, 2001, **105**, 11605–11614.
42. G. Rossi and R. Ferrando, *Nanotechnology*, 2007, **18**, 5706.
43. S. D'Addato, V. Grillo, S. Altieri, R. Tondi, S. Valeri, and S. Frabboni, *Journal of physics. Condensed matter*, 2011, **23**, 175003.
44. K. A. Dick and P. Caroff, *Nanoscale*, 2014, **6**, 3006–21.
45. P. Riello, A. Lausi, J. Macleod, J. R. Plaisier, G. Zerauschek, and P. Fornasiero, *Journal of synchrotron radiation*, 2013, **20**, 194–196.

Nanoscale Accepted Manuscript